Assembling Viral Channel Forming Proteins: Vpu from HIV-1

Li-Hua Li, Hao-Jen Hsu, Wolfgang B. Fischer
Institute of Biophotonics, School of Biomedical Science and Engineering and Biophotonics and Molecular Imaging Research Center (BMIRC), National Yang-Ming University, Taipei 112, Taiwan

Received 15 July 2012; revised 17 October 2012; accepted 22 December 2012
Published online 21 January 2013 in Wiley Online Library (wileyonlinelibrary.com). DOI 10.1002/bip.22210

ABSTRACT:

Different routes of assembly are probed for the transmembrane domain (TMD) of the bitopic membrane protein Vpu from HIV-1. Vpu is responsible for the amplification of viral release from the host cell. The mode of action includes (i) heteroassembly with host factors and (ii) the formation of homo-oligomers, which are able to conduct ions across the lipid membrane. Two different routes of assembling short sequences of the N terminus, including the TMD of Vpu, $Vpu_{1–32}$, and $Vpu_{8–26}$, are presented by using a combination of classical molecular dynamics (MD) simulations combined with a docking approach. The rim of alanines (Ala-8, -11, -15, and -19) resembles an interlocking motif for the sequential assembly into a dimer and trimer. Simultaneous assembly results in oligomeric bundles (trimers to pentamers) with either tryptophans (Trp-23) or purely hydrophobic residues facing the center. Bundles, with serines facing the pore (Ser-24), are energetically not the lowest structures. For pentameric bundles with Ser-24 facing the pore, no water column develops during a short 25 ns MD simulation. © 2013 Wiley Periodicals, Inc. Biopolymers 99: 517–529, 2013.

Keywords: *Vpu HIV-1; membrane protein; assembly; molecular dynamics simulations; docking approach*

This article was originally published online as an accepted preprint. The "Published Online" date corresponds to the preprint version. You can request a copy of the preprint by emailing the Biopolymers editorial office at biopolymers@wiley.com

INTRODUCTION

Many viruses encode integral membrane proteins, which render the lipid membrane permeable for ions and some of them to small molecules.[1–3] The proteins either exist in a bitopic (e.g., M2 from influenza A,[4] Vpu from HIV-1,[5,6] 8a from SARS-CoV[7]) or polytopic form (e.g., p7 from HCV,[8] 2B from entero viruses,[9] and 3a from SARS-CoV[10]). While a structure–mechanism–function correlation is well established for one of these proteins (M2 from influenza A), for most of the other proteins, the correlation is still under debate, especially for Vpu from HIV-1.

Identified as a type I integral membrane protein of 81 amino acids,[5,6] Vpu is found in HIV-1 and related chimpanzee isolate SIV_{CPZ},[11] but not in HIV-2. The protein is classified as an auxiliary protein, since viruses lacking Vpu are still able to replicate to a lower extent[12] (for review see[13–15]). The role of amplification of viral replication is related to two mechanisms, one of which is a down-regulation of several host factors such as CD4,[16] CD317/tetherin/BST-2,[17,18] CD74,[19] and NST-A.[20] Through protein-protein interaction, these proteins are redirected to the ubiquitin-dependent proteasome degradation pathway. For some of these interactions, for example, with CD317/tetherin/BST-2, the transmembrane domain (TMD) of Vpu seems to be essential, for other protein-protein interactions, the phosphorylated cytoplasmic domain (e.g., Vpu–CD4 interaction) is important. The other mechanism is proposed to be driven by the formation of channels via homo-oligomerization

Additional Supporting Information may be found in the online version of this article.

*Present address: Department of Life Science, Tzu Chi University, Hualien 970, Taiwan.
Correspondence to: W. B. Fischer; e-mail: wfischer@ym.edu.tw

Contract grant sponsor: NYMU, the Government of Taiwan
Contract grant sponsor: National Science Council of Taiwan
Contract grant number: NSC98-2112-M-010-002-MY3

into most likely tetramers[21] or pentamers.[21–24] The channels formed are characterized by electrophysiological experiments in which Vpu is expressed in *Xenopus* ocytes.[23,25] In other experiments, the protein is expressed in *Escherichia coli* or human cells lines, purified and reconstituted into artificial lipid bilayers.[23,26] Channel activity has also been confirmed in artificial bilayers when using synthetic peptide fragments which include the TMD of Vpu.[27,28] At this stage channel formation is not univocally correlated to the viral life cycle.

Structural information about Vpu is mainly derived from NMR spectroscopic investigations of protein fragments representing the TMD[29–31] or the cytoplasmic domain,[32–36] with the former identified to be helical (reviewed in[3]). A special feature of the TMD is experimentally found to be a kink around a central amino acid Ile-17.[21] Results from molecular dynamics (MD) simulations of computational models of the TMD suggest a bend spanning from Ile-20 and Ser-24.[37]

Up to now, structural information of a Vpu protein assembly have not been achieved yet and computational methods consequently play an important role in investigating potential assemblies.[38] Computational assemblies are mainly generated by copying a single TMD and aligning the copies around a central axis.[39] Such an approach is guided by featuring a channel in which hydrophilic residues should line a potential ion-conducting pore. In extended protocols, the conformational space of the assembly is screened in a rigid body approach, ranking the assemblies on the bases of a root mean square deviation[40] or on calculation of potential energies.[41,42] During conformational search, each of the helices is "moved" in a concerted fashion. In some protocols, the search of the conformational space is restricted to allow the formation of a ring of serines to be pore lining.[39,40] Recently, an approach has been introduced in which the TMDs of the polytopic channel forming protein 3a from SARS-CoV (severe acute respiratory syndrome – corona virus) are assembled in a sequential, one-after-the-other, approach to propose a channel architecture.[43]

Using a fine grained search protocol,[42,43] the question of whether a sequential build-up forms a pore, is investigated and compared with the previously used concerted protocol in which all TMDs are moved simultaneously to screen the conformational space. The outcomes of the investigations are discussed regarding the putative channel architecture and how this architecture could be obtained in vivo.

RESULTS

$Vpu_{1–32}$ is embedded into a hydrated lipid bilayer patch at various positions along the bilayer normal. Calculation of the RMSD values for each of the simulations, result in fluctuations around 0.3 nm for two of the simulations, $VpuI_{1–32}$ and $VpuII_{1–32}$, and around 0.5 nm for a third one $VpuIII_{1–32}$ (Figure 1A, I). Simulation of a shorter sequence solely composed of the TMD, $Vpu_{8–26}$, results in RMSD values fluctuating around 0.1 nm after a large rise up to 0.3 nm during the first 30 ns (Figure 1A, II). One of the two $Vpu_{1–32}$ simulations with fluctuating RMSD values of around 0.3 nm shows a *w*-shaped RMSF distribution with a maximum fluctuation around Ala-15, which is centered in the core of the bilayer (Figure 1A, II, black curve). The values from the other two simulations start with lower values at the N terminal side and increase over the entire stretch of the helix reaching their highest values around Trp-23 (Figure 1A, II). Residues Ile-25 to Ile-28 show low values, which increase again toward the remaining C terminal residues. The RMSF values for the amino acids in $Vpu_{8–26}$ increase from Val-13 to Trp-23 (Figure 1B, II).

The 100 ns simulations of $Vpu_{1–32}$ result in larger tilts for the helices (Figures 2A–2C and Table I) than the simulations of $Vpu_{8–26}$ (Figure 2D). Whilst the values for $Vpu_{1–32}$, I–III are calculated to be 18.9 ($\pm$5.9)°, 13.1 ($\pm$6.8)°, and 39.4 ($\pm$3.1)° the value for $Vpu_{8–26}$ is around 9.4 ($\pm$4.3)° (Table I). The kink angles for $Vpu_{1–32}$ are calculated to be 150.8 ($\pm$11.0)°, 169.4 ($\pm$1.2)°, and 150.3 ($\pm$21.5)° and 157.3 ($\pm$5.2)° for $Vpu_{8–26}$ (Table I). Inspection of the structures after 100 ns reveals that the larger tilt for the longer helices ($Vpu_{1–32}$) results from "reintegration" of residues into the head group region of the bilayer (Figure 2) at either ends. Due to the short sequence in $Vpu_{8–26}$ such a rearrangement is not necessary. $Vpu\text{-}II_{1–32}$ shows the largest conformational change in as much as 8 residues (Ile-25–Lys-32) are embedded into the head group region. The large conformational change is reflected in the large RMSD values. Residues Ile-25 to Lys-32 is not considered in the calculation of the kink and tilt angles. $VpuI_{1–32}$ adopts the lowest tilt and shows structural integrity. This structure, hither forth called $Vpu_{1–32}$, and $Vpu_{8–26}$ are usedto conduct further calculations.

Sequential Assembly

Both dimers of $Vpu_{1–32}$ (Figure 3A, I) and $Vpu_{8–26}$ (Figure 3B, I), allow the rim of alanines (Ala-8, -11, -15, and -19) of one of the helices to face the opposing helix when assembled. The residues on the opposing helices are Val-13, -14, and -21. $Vpu_{1–32}$ assembles with an interhelical distance of 13.4 Å and a tilt of 12° of one helix in respect to the other whilst $Vpu_{8–26}$ assembles with an interhelical distance of 9.4 Å and a tilt of 28° (Table II). Inspection of the energy data versus the tilt angle shows that very low energy structures for $Vpu_{8–26}$ are found with tilts of −24° and 28° with similar rotational angles (Supporting Information Figure 1B, boxed).

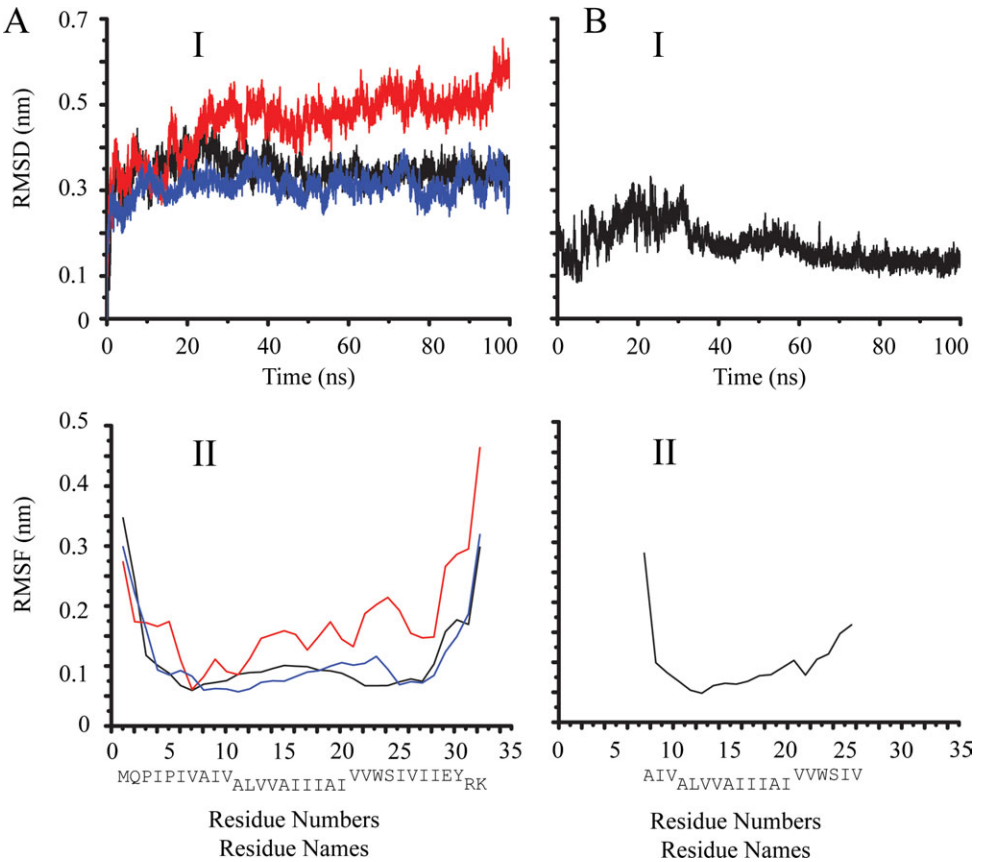

FIGURE 1 Root mean square deviation (RMSD) of the Cα atoms of three TM peptides containing the first 32 amino acids of Vpu (HV1H2), $Vpu_{1–32}$, and the respective RMSF of the residues based on the Cα atoms (A). The three different runs are colored as black, red, and blue, with the first used for the assembly. RMSD and RMSF values for the shorter Vpu peptide, $Vpu_{8–26}$, are shown in (B).

Generating the dimer, trimer, and tetramer, the $Vpu_{1–32}$ helices pack onto the alanine rim of another helix in the assembly (arrows in Figure 3A, II and III) facing the helix side with the valines. The additional fifth helix still points its valines toward the tetramer but does not match with the alanine-rim (Figure 3A, IV). For $Vpu_{8–26}$, mostly the site of the valines attach to each other to form the bundles (Figure 3B, II–IV). For the pentamer formation, the alanine rim of the attaching helix faces the bundle (Figure 3B, II–IV).

Inspection of the graphs, energy versus rotational angle, reveals that the low energy valleys for $Vpu_{1–32}$ are separated by barriers between ∼40 and ∼100 kcal/mol (Figure 4A, I–IV). The valleys for $Vpu_{8–26}$ are separated by barriers increasing from 30 kcal/mol in the dimer, over 60 kcal/mol in the trimer and to larger than 100 kcal/mol in the tetramer and pentamer (Figure 4B, I–IV). Helices are added with a positive tilt angle except for the helix $Vpu_{1–32}$ forming the trimer and the pentamer (Table II).

The shorter helices, $Vpu_{8–26}$, adopt an energetically more favorable locking-into-groove pattern than the longer helices, supporting the concept that the driving motive for assembly is given by the TMD. From visible inspection, all tetrameric assemblies look as if to form a symmetrical bundle, which could eventually emerge into a channel-like formation (Figures 3A and 3B, III). Especially the $Vpu_{8–26}$ tetramer shows all helices with the alanine-rim facing the outside of the bundle (Figure 3B, III).

Short MD simulations of 20 ns are applied to assess the integrity of the tetrameric bundles, which are obtained from the sequential assembly (Figure 5). The RMSD of both tetramers, $Vpu_{1–32}$ and $Vpu_{8–26}$, are low. The values for the RMSF of the individual helices show a continuous increase of the values for all helices of $Vpu_{1–32}$ and a *w*-shape for all helices of $Vpu_{8–26}$ (Supporting Information Figure 2). The formation of pores with serines pointing into the lumen of the pore has not been achieved within 20 ns MD simulation.

Table I Tilt and Kink Angles Calculated from MD Simulations for the Individual Helices Vpu1–32 and Vpu8–26 as well as the Individual Helices in the Tetrameric and Pentameric Assemblies

	Monomer				Tetramer		Pentamer			
	$VpuI_{1–32}$	$VpuII_{1–32}$	$VpuIII_{1–32}$	$Vpu_{8–26}$	$Vpu_{1–32}$	$Vpu_{8–26}$	$Vpu_{1–32}$	$Vpu_{1–32}$ ser	$Vpu_{8–26}$	$Vpu_{8–26}$ ser
Tilt (°)	18.9 ± 5.9	13.1 ± 6.8	39.4 ± 3.1	9.4 ± 4.3	11.9 ± 2.8	11.0 ± 4.2	24.9 ± 4.6	20.2 ± 4.1	21.9 ± 4.8	8.7 ± 4.3
					11.1 ± 2.4	11.0 ± 4.2	17.2 ± 3.0	24.0 ± 4.8	20.5 ± 4.8	17.0 ± 3.8
					16.5 ± 2.1	15.8 ± 5.3	13.5 ± 3.2	20.3 ± 5.6	32.0 ± 5.4	7.4 ± 3.8
					10 ± 72.8	12.6 ± 5.4	15.9 ± 3.3	12.0 ± 3.3	24.8 ± 4.9	23.0 ± 5.7
							16.4 ± 3.1	9.1 ± 2.0	27 ± 14.6	20.4 ± 11.1
Kink (°)	150.8 ± 11.0	169.4 ± 1.2	150.3 ± 21.5	157.3 ± 5.2	166.3 ± 3.5	151.9 ± 7.9	165.4 ± 5.4	149.1 ± 11.9	166.3 ± 3.9	156.2 ± 6.1
					163.7 ± 12.7	160.5 ± 4.8	161.5 ± 5.7	167.5 ± 4.7	166.4 ± 5.7	166.4 ± 6.1
					167.1 ± 5.7	163.9 ± 3.7	163.3 ± 4.1	162.1 ± 5.2	158.4 ± 4.2	168.4 ± 5.7
					162.7 ± 7.7	155.2 ± 4.2	161.3 ± 5.5	161.4 ± 5.6	165.2 ± 4.7	166.6 ± 4.2
							163.4 ± 4.5	153.2 ± 6.5	164.8 ± 4.8	159.8 ± 8.9

"I"–"III" refer to the naming in Figure 2. "ser" marks the assembly with serines facing the lumen of the pore.

Simultaneous Assembly

Simultaneous alignment of the helices delivers more tightly packed bundles, indicated by lower interhelical distances, than the ones found for the sequential assembly (Figures 6A and 7A, and Table II). Whilst $Vpu_{1–32}$ assembles into positively tilted bundles, for example, 6° (trimer), 26° (tetramer), 16° (pentamer), $Vpu_{8–26}$ assembles into negatively tilted bundles, for example, −30° (trimer), −36° (tetramer), and −16° (pentamer). All lowest energy bundles have a conformation in which either all Trp-23 residues face the pore or the hydrophobic side including the alanine rim as in the $Vpu_{1–32}$ tetramer. The trimer of $Vpu_{8–26}$ is the only bundle, which allows Ser-24 to point toward the center of what could become a pore. Highlighting the lowest energy structures of bundles with serines facing the pore, it is evident that the tilt and also the handedness only reverse in the tetrameric bundles for both $Vpu_{1–32}$ and $Vpu_{8–26}$ (Figures 6B and 7B). Whilst interhelical distances remain nearly the same as for the lowest energy structures, as expected, the rotational angles differ by more than 120° in some cases.

Short 20 ns MD simulations of the pentameric assemblies do not allow the bundles to develop into water filled pores (Figures 6A and 7A, lower panels) albeit stable RMSD values and RMSF values showing the same pattern as mentioned above (Supporting Information Figure 3). The low energy bundles with the serines facing the pore allow for a water filled pocket at the C terminal side (Figures 6B and 7B, lower panels). After about 20 ns MD simulations the water pocket disappears and the circular structure of the bundle vanishes. In one of the simulations one of the Trp-23 is moving out of the pore by tilting the respective helix (Figure 7A, lower panel). A rotational motion is not observed.

With an increasing number of helices forming the bundle, the rotational energy barriers separating the groves increase with increasing number of helices (Figure 8). The values increase to about 120 kcal/mol for the $Vpu_{1–32}$ trimer (about 50 kcal/mol for $Vpu_{8–26}$), to more than 200 kcal/mol for the $Vpu_{1–32}$ tetramer (about 100 kcal/mol for $Vpu_{8–26}$) and about 450 kcal/mol for the $Vpu_{1–32}$ pentamer (about 300 kcal/mol for $Vpu_{8–26}$). Still, this does not prevent the bundles from moving translationally and losing their bundle shape (Figures 6 and 7). The lowest energy structures are not in the same rotational low energy valleys as the low energy structures with serines facing the pore. Translational motion and tilt (see Table II) allow large rearrangements of the assembled helices, albeit being rotationally restricted.

DISCUSSION

Viral channel forming proteins are thought to be manufactured at and released into the endoplasmic membrane. As a

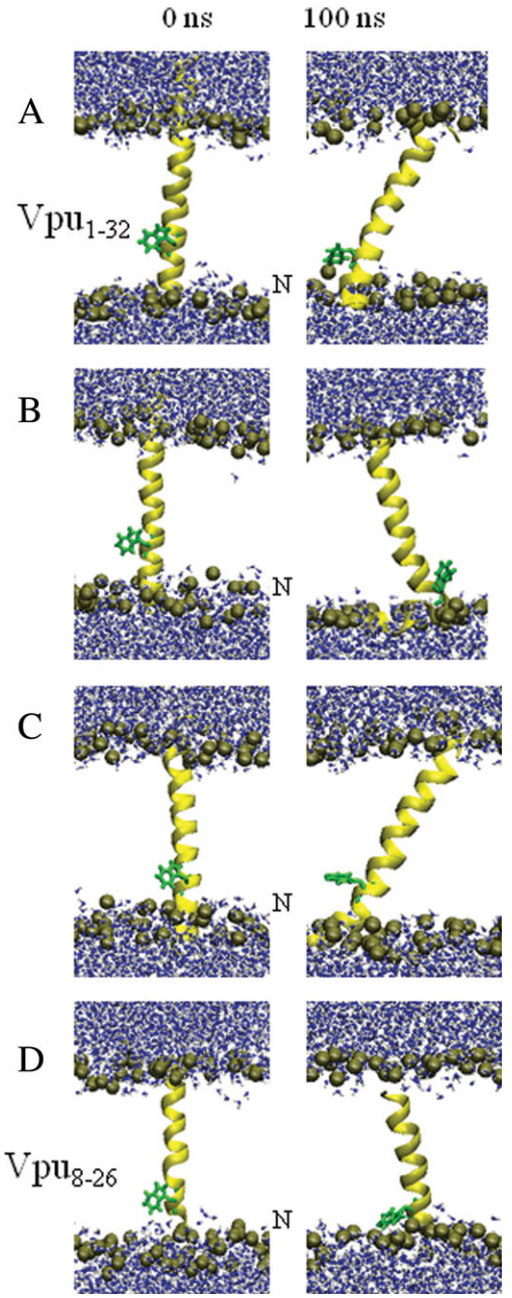

FIGURE 2 Graphical representation of the simulations of the individual TM peptides $Vpu_{1–32}$ (A–C) and $Vpu_{8–26}$ (D). Structural models refer to the black (A, D), red (B), and blue (C) curves in Figure 1. The backbone of the helices is shown in yellow with tryptophans marked in green, using a stick modus. The lipid molecules are omitted for clarity and only the positions of the phosphate atoms are highlighted as dark spheres. Water molecules are shown in ball-stick modus with the oxygen atoms in blue and hydrogen atoms in white. The N terminus is marked.

follow-up event it is anticipated that the protein needs to diffuse within the membrane to assemble into functional channels with integral membrane proteins of the same kind. The following steps of this process are computed: (i) relaxation of the structure within the membrane, which is seen to be the equivalent of relaxation and diffusion from the site of production to the site of assembly; (ii) assembly of the bundle structure and; (iii) consequent relaxation of the bundle structure within the membrane as it is routed to its final destination. Whilst the relaxation is done by applying MD simulation, the assembly is conducted by using a docking approach. The docking approach allows to collect time-independent "snapshots" of potential structures. Since a "symmetric" assembly around a central axis is difficult to envision in vivo if

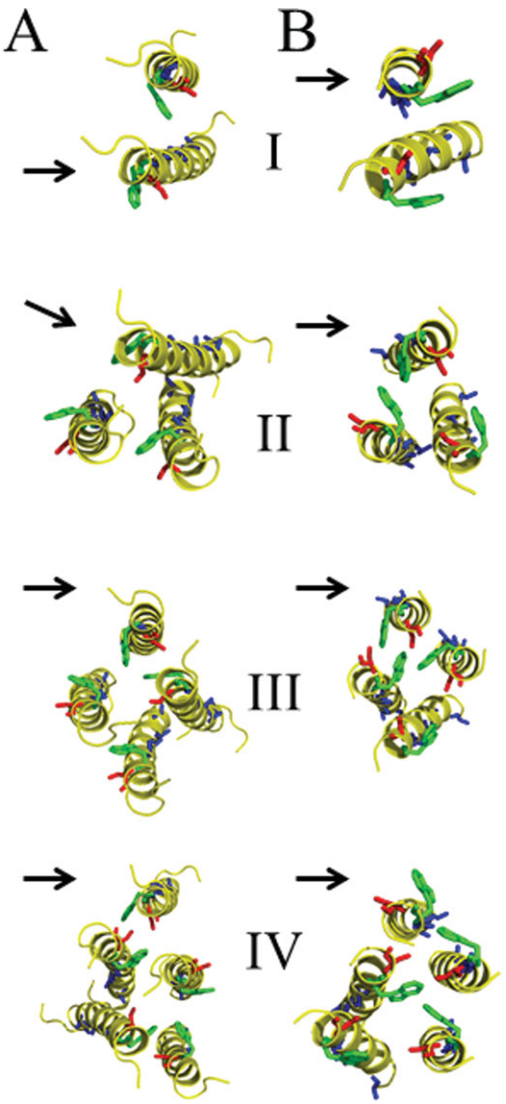

FIGURE 3 Graphical representation of sequentially assembled $Vpu_{1–32}$ (A) and $Vpu_{8–26}$ (B) starting with a dimer (I), followed by a trimer (II), tetramer (III), and pentamer (IV). The helices are shown in yellow. The following amino acids are highlighted in stick modus: tryptophans (green), serines (red), and alanines (blue). The view is from the C to the N terminus. Arrows indicate the helix added.

Table II Distances in Å, Tilt, and Rotational Angles as well as the Energy Values in kcal/mol for the Lowest Energy Structures Identified in the Assembly Protocols

		Distance (Å)		Tilt (°)		Rot-Angle (°)		*E* (kcal/mol)	
		Seq	Sim	Seq	Sim	Seq	Sim	Seq	Sim
Dimer	Vpu_{1-32}	13.4		12		80		−790.0	
	Vpu_{8-26}	9.4		28		216		−341.1	
Trimer	Vpu_{1-32}	13.8	9.25/9.25	−32	6/0	56	60/140	−1323.5	−1180.8/−1105.4
	Vpu_{8-26}	10.2	8.0/7.8	32	−30/−30	256	30/10	−571.2	−402.7/−364.4
Tetramer	Vpu_{1-32}	12.2	11.8/10.8	16	26/−6	72	320/180	−1855.5	−1606.1/−1429.1
	Vpu_{8-26}	10.9	8.5/9.0	8	−36/12	64	290/4	−778.1	−635.4/−549.4
Pentamer	Vpu_{1-32}	13.8	12.3/13.8	−8	16/18	112	125/170	−2320.1	−2285.6/−2022.7
	Vpu_{8-26}	11.5	10.8/11.3	−16	−16/−4	48	355/75	−815.6	−961.5/−885.7

"Seq" and "Sim" stand for sequentially and simultaneously, respectively, assembled structures. Values separated by "/" represent the data for the lowest structure (value/) and the lowest structure with serines facing the lumen of the pore (/value). Rotational Angle (Rot-Angle) describes the rotation of the "moving" helix along the helix axis.

only "free" diffusion is allowed, a sequential built-up of a putative bundle is considered as well.

The architectural concept of an ion or substrate conducting pore is that hydrophilic residues line the lumen of the pore to lower the dielectric barrier for water molecules passing through the pore. Experimental evidence for the concept has been given from molecular biological experiments[44] and recently confirmed in structural models of ion channels such as GLIC and ELIC.[45,46] A series of computational assembly protocols have been reported in the literature to generate bundles of Vpu and to evaluate their structural integrity and ion conducting properties.[39,47–49]

Computational and Experimental Modeling of Bundles of Vpu

In reference to experimental evidence from FTIR spectroscopy using a Vpu_{1-31} peptide,[41] left-handed Vpu assemblies with tryptophans,[39] and alanines[50] facing a putative pore in a pentameric and a hexameric[50] assembly have been proposed. The general feature of reports of computational data is that the Vpu bundles expel water and do not stay in a channel like shape.[50] The data for a pentameric assembly propose a conical shape with a restriction toward the C terminal side.

From solid-state NMR spectroscopic analysis, controversial models of the bundles are proposed. On the one side right-handed tetrameric, pentameric and hexameric bundles with Ile-17 pointing into the pore and outward facing tryptophans are suggested.[21,51] On the other side, using orientation restraint potentials from one of the above mentioned solid-state NMR spectroscopic measurements recorded with a Vpu_{2-30+} peptide[21] data are reported, which allow the modeling of left-handed tetrameric and pentameric bundles over right handed bundles with tryptophans pointing into the pore.[52] Here "+" stands for an additional GGKKKK motif, which has been added to ease the purification of the peptide. More distance measurements would be necessary to narrow down this issue.

In respect to the number of helices forming a bundle, all NMR data have in common that they allow the assumption that several oligomers exist within the lipid membrane. It is therefore possible, that Vpu does not adopt a single oligomeric state. Based on a gel permeation analysis, Vpu has been suggested to exist in equilibrium between monomers and pentamers.[24] This result runs parallel with findings for other channels such as p7 from Hepatitis C virus, which is reported in a hexameric[53,54] and heptameric assembly.[55]

Taken together, experimental findings for a hydrophobic core of the assembly rather than a pore guided by hydrophilic residues are evident. In addition to that, all the reports are not specific about the oligomerization state, they are rather proposing the protein to be present in multiple assembly states. There is no decisive opinion about the handedness, yet. It seems that handedness varies in dependence of the experimental conditions.

Single Helices: Structure, Kink, Tilt, and Bend

The RMSF data of a 100 ns MD simulation of single Vpu_{1-32} match experimental findings[21] in as much as Ala-15 within the core region exhibits a maximum RMSF value in one of the simulations (e.g., Figure 1A, II, black line). Since the maximum is broad, Ile-17 also shows high values. Together with earlier simulations in which the kink is identified to be between Ile-20 and Ser-24[37] the region between Ala-15 and Ser-24 marks a flexible region, which rather induces a bend than a sequence-specific kink. This finding is though contrary to some NMR spectroscopic data,[56] which do not

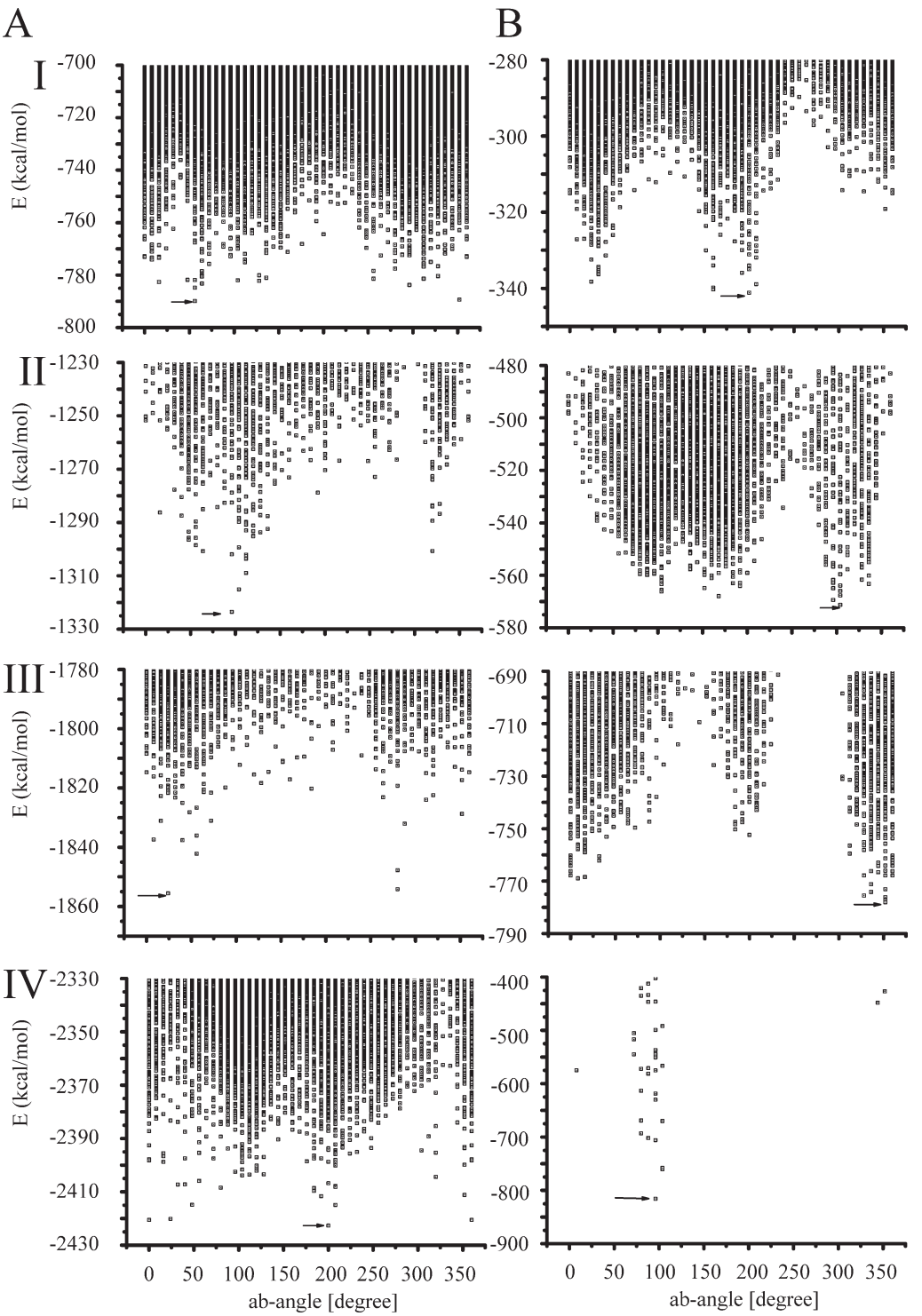

FIGURE 4 2D energy plots for the sequentially assembled $Vpu_{1–32}$ (A) and $Vpu_{8–26}$ (B). The plots resemble energy versus the angle between two helices (I), and the angle between the assembled structure and the newly posed helix (II–IV). Arrows mark the lowest energy structure. Assembly is achieved using the protocol in MOE (see Materials and Methods).

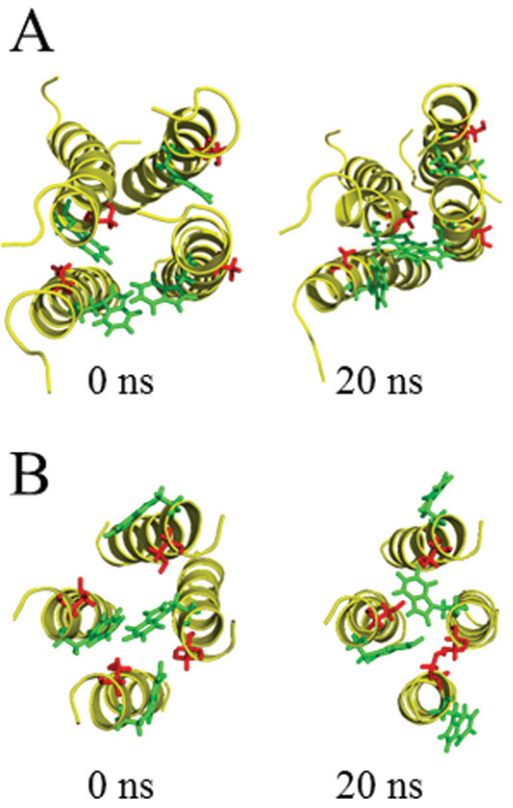

FIGURE 5 Graphical representation of sequentially assembled tetrameric $Vpu_{1–32}$ (A) and $Vpu_{8–26}$ (B) taken from a MD simulation at the beginning (0 ns) and the end (20 ns). Lipid and water molecules are omitted for clarity and the bundle is shown with the helical backbone in yellow, tryptophans, and serines in green and red, respectively. The view is from the C to the N terminus.

report any kinks or bends in their structures. Possibly, kink and bends depend on the oligomeric state of the peptide or protein.

Bundles

In a previous study[42] using $Vpu_{8–26}$, several pentameric bundle structures are presented in which the lowest energy structure adopts a conformation in which Trp-23 facing the pore. Four more low energy structures are highlighted in the previous study, which are found in rotationally distinct energy valleys. Only one of the low energy structures allows for a conformation with Ser-24, facing the lumen of the pore. The tilt angles of the five models do not reflect any preference for either handedness of the bundle. From plotting the energy values either versus the rotational or tilt angles, it is suggested, that gating rather occurs to a sliding/tilting motion than to a rotational one. Assembling $Vpu_{1–32}$ also results in a lowest energy structure with Trp-23 facing the pore and several other low energy structures with Ser-24 located at the helix-helix interface and not pointing into a pore.[57]

This study shows similar results for the pentameric assembly as mentioned above. These results also allow the statement, that the lowest energy structures in trimers and tetramers do not allow Ser-23 facing the pore. The "ideal" structures with Ser-23 facing the pore are energetically distinct from the lowest structures. The AMBER 94 force field is treating the aromatic residues specifically,[58] which makes the lowest energy structures, shown in this study, reasonable models. It is evident from the data that an increasing number of helices result in narrow energy valleys, making rotational motions more and more unlikely. However, the minimum energy values within these valleys are the same within narrow margins.

Handedness only seems to be uniform for multiple assembly states if a simultaneous assembly protocol is used. The differences in handedness between the lowest energy structures of $Vpu_{1–32}$ (left-handed) and $Vpu_{8–26}$ (right-handed) may be reflected by the computational protocol used. The protocol is a docking type search of the conformational space. The results are dependent on the amino acid sequence, which includes the EYR motif in $Vpu_{1–32}$, and the initial orientation of the backbone. In the overall search protocol, the opposite handedness is also observed albeit at higher energies. It has been reported, that handedness switches from left to right and back during coarse grained MD simulations of a dimeric peptide, for example, WALP23.[59] Further energetic and dynamic studies are necessary to evaluate whether the hinge region between the TMD and the cytoplasmic domain allows rotational freedom of the TMD, independent from the cytoplasmic domain[56] and, whether switching handedness is a structural feature in the mechanism of function of this protein. Sequential build-up of the bundles ends up in arbitrarily tilted helices, and bundle conformations different from those obtained with the simultaneous assembly protocol.

Gating

From a closed low energy structure to an open higher energy structure, which allows the existence of a column of water, the protein bundle needs to rotate and thereby crosses large energy barriers. A sliding along each other and changing the tilt does not impose similarly large barriers. Of course the question, where to take the energy from for any of the proposed movements, still remains. A potential across the membrane could deliver the relevant energy for conformational changes, allowing gating. It is also possible, that an involvement of rafts can play a role in positioning Vpu in a proper way.[60]

Sequential Assembly

In the sequential assembly, hydrophobic matching dominates the orientation of the helices within the assemblies. It seems

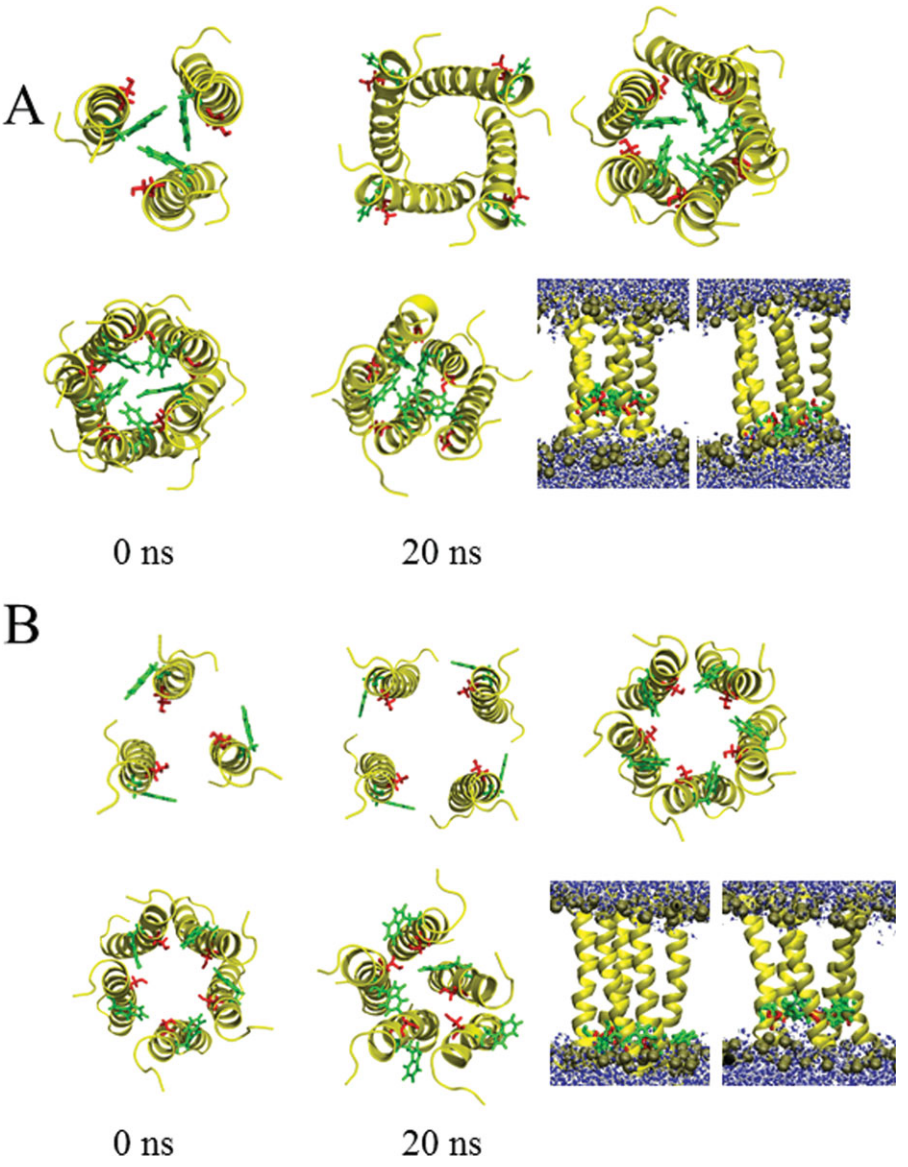

FIGURE 6 Models of simultaneously assembled Vpu_{1-32} is shown as lowest structure due to the MOE assembly (I) and the lowest structures, which show the serines to face the lumen of the pore (II). The bundles in the upper row of each panel are shown from left to right as trimers, tetramers, and pentamers derived from the assembly protocol. The bundles in the lower row of each panel represent the structures at 0 and 20 ns of the MD simulation in a top view, as well as the side view. The color coding is backbone helices in yellow, tryptophans in green, serines in red, water molecules with oxygen atoms in blue, and hydrogen atoms in white. The lipid molecules are omitted for clarity and only the positions of the phosphate atoms are highlighted as dark spheres.

as if, the van der Waals interactions[61] and steric optimized complementary matching play the dominant role in the assembly. The single serine within the otherwise hydrophobic stretch compensates its demand for a hydrogen bond acceptor by interacting perfectly with the next available carbonyl group, within the same helix. Examples for complementary matching have been shown in coarse grained simulations.[61–65] In general, it is noted that a small difference in energy make two partners weak or strong binders within the lipid bilayers.[66]

Biological Implications

With the current assumptions at hand the "channel" should eventually be voltage gated, which has not been found to

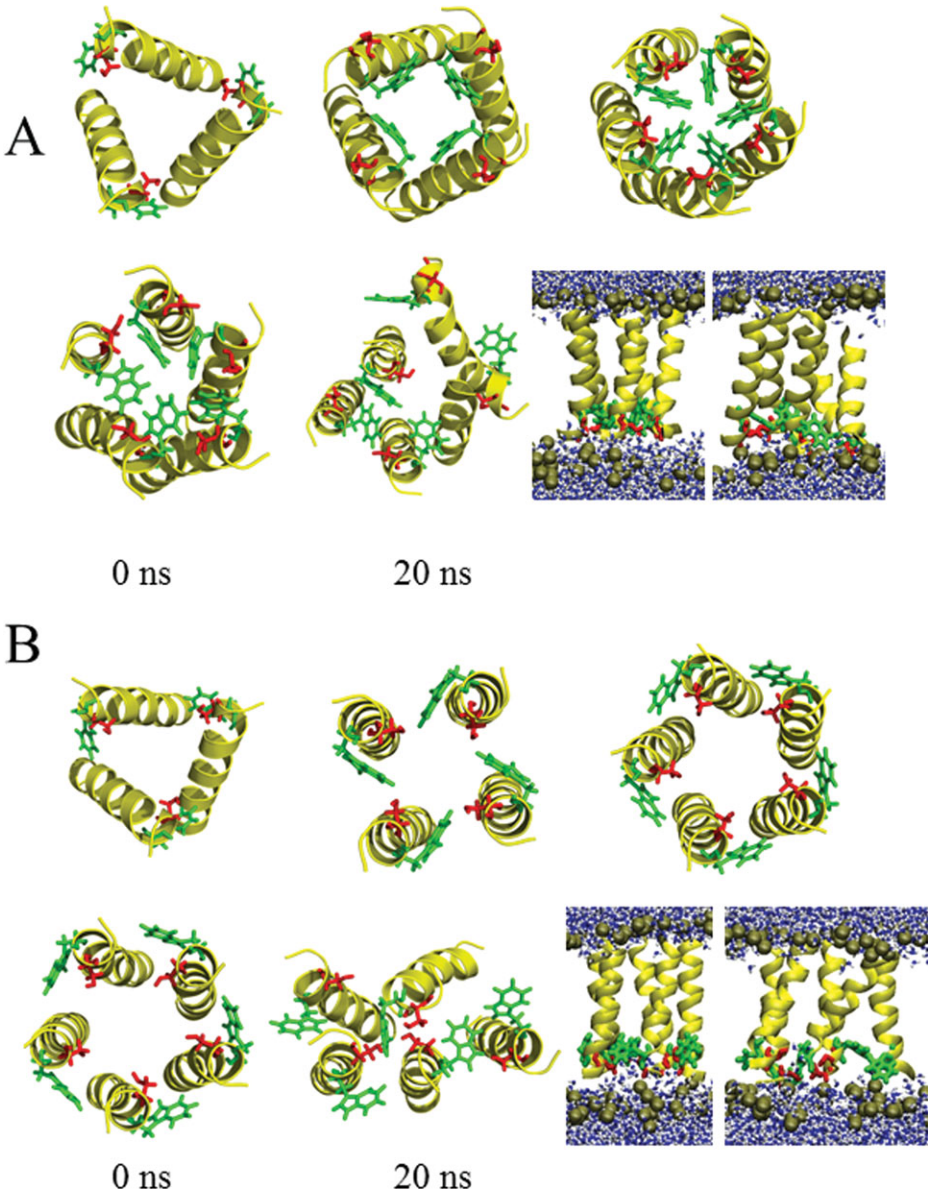

FIGURE 7 Models of simultaneously assembled Vpu_{8-26} is shown as lowest structures due to the MOE assembly (I) and the lowest structures, which show the serines to face the lumen of the pore (II). The bundles are organized as described in Figure 6.

date. Another route to "force" some of the Vpu proteins into a "proper" assembly would be to impose conformational restraints throughout raft attachment.[60] A sequential built up, which is a possible route driven by free diffusion seems not necessarily to be delivering a pore like structure. Much more arrangements and constraints need to be imposed, to generate a somehow circular shaped bundle.

With lowest energy structures forming a hydrophobic pore, the bundle should be unselective, which matches experimental data.[23,28] Computational evidence report that hydrophobic pores allow at least water to permeate.[67,68]

At this state of investigation, Vpu is in the focus because of its role of attaching to other host membrane proteins. If the tryptophans are pointing inside an assembly, the alanine rim, a potential site for protein–protein interaction,[69] is exposed to the outside. In a sequential assembly, this interaction site is still exposed to the "outside." Consequently, bundle and non-bundle structures could deliver conformations for Vpu-host interactions. Binding to a host factor could then be energetically more favorable than staying in an ensemble with other Vpu proteins. Thus, an equilibrium between assembled and host-Vpu complexes could exist. It is

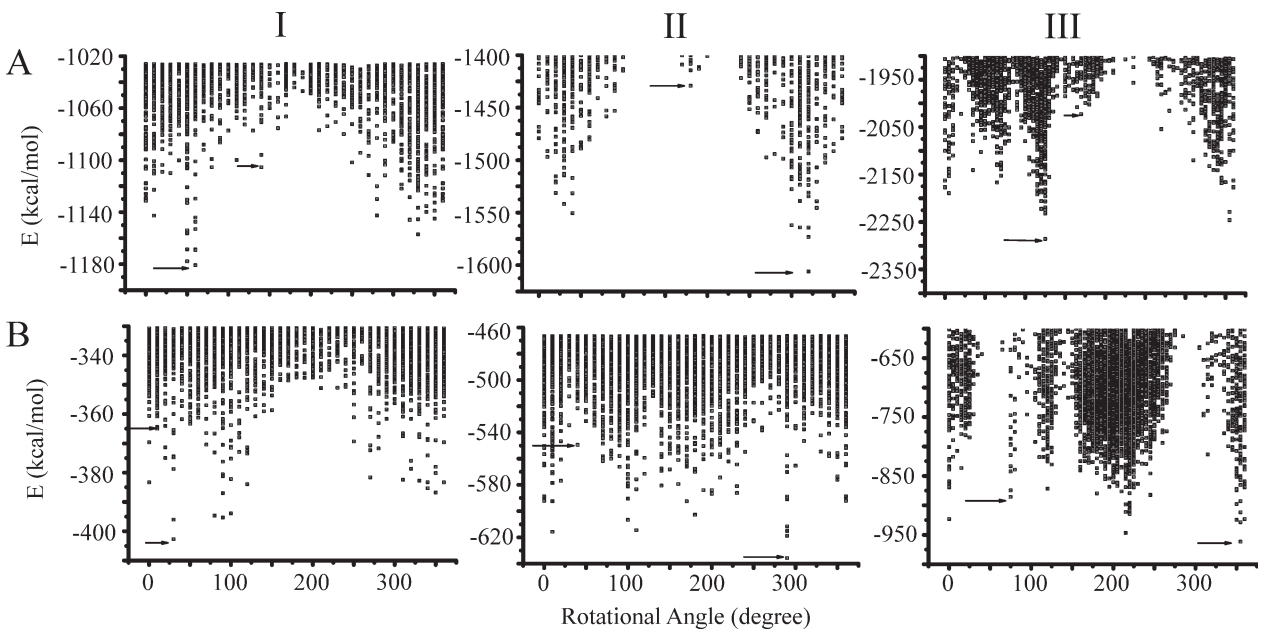

FIGURE 8 2D energy plots for the simultaneously assembled $Vpu_{1–32}$ (A) and $Vpu_{8–26}$ (B). The plots resemble energy versus the rotational angle around the helix long axis of the trimer (I), tetramer (II), and pentamer (III). Arrows mark the lowest energy structure and the lowest structure with serines facing into the lumen of the pore. Assembly is achieved using the protocol in MOE (see Materials and Methods).

up to further investigations to find out, how the Vpu-Vpu as well as the Vpu-BST-2 interactions competes with each other.

CONCLUSIONS

Assemblies of Vpu, independent on the starting conditions and peptide length, result in pores occluded by tryptophans or being mantled by hydrophobic residues. Experimental and computational evidence of handedness is not congruent and the amino acids involved in a putative kink or bend are not identified univocally.

Based on the difficulties to address the assembly state, it may be concluded that there are oligomers of Vpu, existing in "patches." The patches do not adopt a single defined conformational state. It may be, that the different oligomeric states exist in a dynamic equilibrium. Handedness (right or left) could be irrelevant for function.

Thus, Vpu may rather act in a bandwidth of possible geometries and assemblies. Some of the assemblies are in a state to allow for interaction with membrane proteins of the host and some of them to enable ion conductance as a hydrophobic/hydrophilic pore.

Still an open question is what drives the patch ("swarm") to allow specific members to break out and adopt a particular "functional state." Still to be evaluated is how much lipid rafts effect the formation of assemblies. The idea, that a single functional structure is responsible for the mechanism of function may be corrected into the statement that a distribution of functional structures may exist for the Vpu monomer. This distribution is the basis for the multi-tasking ability of this protein. Remaining in a flexible state at all structural levels, even the quaternary structure, may probably be an essential feature as long as no highly selective or specific mechanism of function is needed. In respect to the ability to form channels, lowering electrochemical gradients in an almost time independent and spatially not well defined place within the cell, does not need a tool, here on a quaternary level, which is structurally highly specific.

MATERIALS AND METHODS

Ideal helices ($\phi = -65°$, $\psi = -39°$) of the N terminal side of Vpu (Vpu HV1H2) including the TMD of the protein were generated using the program MOE2008.10 (Molecular Operation Environment, www.chemcomp.com):

$Vpu_{1–32}$: MQPIPIVAIV^{10} ALVVAIIIAI^{20} VVWSIVIIEY^{30} RK,
$Vpu_{8–26}$: IV^{10} ALVVAIIIAI^{20} VVWSIV

Preparation of the Protein/Lipid/Water System

Proteins, uncharged at both ends, were embedded into POPC lipid bilayer patches (POPC: 16:0-18:1 diester PC, 1-palmitoyl-2-oleoyl-*sn*-glycero-3-phosphocholine). Prior to protein insertion, patches of

128 and 288 lipids were equilibrated for 70[37] and 50 ns, respectively, and used for the simulations.

Individual helices and protein assemblies were individually inserted into the POPC bilayer patches using the MOE software package. Lipids were manually removed, so that overlapping with the proteins was avoided. Finally, the patches consisted of 122 lipids (6344 atoms) for the monomeric helices and 244 lipids for the assemblies (trimers, tetramers, and pentamers). The protein/lipid system was hydrated with about 3655 (122 lipids) and 8746 (244 lipids) water molecules.

All MD simulations were carried out using GROMACS 4.0.5 with the Gromos96 (ffG45a3) force field. Peptides, lipids, and the water molecules were separately coupled to a Berendsen thermostat at 310 K with a coupling time of 0.1 ps. The compressibility was set to 4.5e-5 bar^{-1}. The monomers were simulated with a semi isotropic pressure coupling scheme, whilst for the assemblies, a surface-tension coupling scheme was used. Long range electrostatics were calculated using the particle-mesh Ewald (PME) algorithm with grid dimensions of 0.12 nm and interpolation order 4. Lennard-Jones and short-range Coulomb interactions were cut off at 1.4 and 0.9 nm, respectively. Water molecules were represented by the SPC model. The protein/lipid/water system was energy-minimized (1000 steps steepest descents, 5000 steps of conjugate gradient) followed by 1.9 ns (122 lipid patch) and 15 ns (244 lipid patch) of equilibration MD simulation. The following equilibration protocol was used: (i) the temperature was gradually increased from 100 to 200 K and 310 K. The system was run for 200 ps for the first two temperatures and 1.5 ns for the latter (500 ps for the patch containing 122 lipids). During these simulations the protein remained fully restraint (k = 1000 kJ mol^{-1}). At 310 K the restraints kept on the protein were released in 4 steps from k = 500 kJ mol^{-1} nm^{-2} to k = 250 kJ mol^{-1} nm^{-2}, k = 100 kJ mol^{-1} nm^{-2}, and finally k = 25 kJ mol^{-1} nm^{-2}; each step was run for 1.5 ns. For the system containing 122 lipids, 2 steps (k = 500 kJ mol^{-1} nm^{-2} and k = 250 kJ mol^{-1} nm^{-2}) were used, each running for 500 ps.

Assembly

For the assembly, an average structure of the backbone residues of the individual helices based on a PCA calculation, as reported earlier,[42] was undertaken using the program g_covar from the GROMACS-4.0.7 package. In brief, the structures of the last 10 ns of each simulation were averaged over the first few eigenvectors. Rotational and translational movements of the helices were canceled out by fitting each of the consecutive helix structures to the first structure.

The monomers were assembled using a program based on the inscriptive language with a protocol reported earlier.[42] The AMBER 94 force field was used for energy calculations. To simulate the assembly within the lipid bilayer the dielectric constant (ε) was set as ε = 2. The helical backbone structures were aligned along the z-axis. Two assembly protocols were used: a simultaneous protocol[42] and a sequential protocol.[43] In the first protocol, the helices were copied and positioned around a central axis (C2, C4, or C5 symmetry) and aligned. In the latter protocol, the respective "new" helices were assembled onto afore assembled helices. The sampling of the conformational space is computed along the distance of the helices towards the central axis, the tilt and two rotational angles of the helices. Vpu dimers were generated by screening the interhelical distance in steps of 0.25 Å, the tilt and rotational angles in steps of 2° and 5°, respectively. Interhelical distances between 10 and 15 Å for $Vpu_{1–32}$ as well as 9.0 and 11.6 Å for $Vpu_{8–26}$ were sampled. The tilt was varied between ± 36°. The assembly protocol usually generated about 350,000 conformers, which were stored in a database for further analysis.

Plots of the root mean square fluctuation (RMSF) of the Cα atoms of each residue as well as calculations of the tilt and kink angles were generated over the last 70 ns of the 100 ns simulation and over the entire duration of the 20 ns simulation run. The tilts and kinks are measured over the center of mass of the backbone of residues 5–8, 20–23, and 24–28.

The simulations were prepared on a DELL T7500 workstation and submitted to the National Center for High Performance Computing (NCHC), Hsinchu, TW using 8 cpu's in parallel for the production run. Plots and pictures were made with VMD-1.8.7 and Origin8.

The authors acknowledge the National Center for High-Performance Computing (NCHC), TW, for providing computer time and service.

REFERENCES

1. Fischer, W. B.; Sansom, M. S. P. Biochim Biophys Acta 2002, 1561, 27–45.
2. Gonzales, M. E.; Carrasco, L. FEBS Lett 2003, 552, 28–34.
3. Fischer, W. B.; Wang, Y.-T.; Schindler, C.; Chen, C.-P. Int Rev Cell Mol Biol 2012, 294, 259–321.
4. Lamb, R. A.; Zebedee, S. L.; Richardson, C. D. Cell 1985, 40, 627–633.
5. Strebel, K.; Klimkait, T.; Martin, M. A. Science 1988, 241, 1221–1223.
6. Cohen, E. A.; Terwilliger, E. F.; Sodroski, J. G.; Haseltine, W. A. Nature 1988, 334, 532–534.
7. Chen, C.-Y.; Ping, Y.-H.; Lee, H.-C.; Chen, K.-H.; Lee, Y.-M.; Chan, Y.-J.; Lien, T.-C.; Jap, T.-S.; Lin, C.-H.; Kao, L.-S.; Chen, Y.-M. A. J Infect Diseases 2007, 196, 405–415.
8. Lin, C.; Lindenbach, B. D.; Pragai, B. M.; McCourt, D. W.; Rice, C. M. J Virol 1994, 68, 5063–5073.
9. van Kuppeveld, F. J.; Galama, J. M.; Zoll, J.; Melchers, W. J. J Virol 1995, 69, 7782–7790.
10. Lu, W.; Zheng, B.-J.; Xu, K.; Schwarz, W.; Du, L.; Wong, C. K. L.; Chen, J.; Duan, S.; Deubel, V.; Sun, B. Proc Natl Acad Sci USA 2006, 103, 12540–12545.
11. Huet, T.; Cheynier, R.; Meyerhans, A.; Roelants, G. Nature 1990, 345, 356–359.
12. Klimkait, T.; Strebel, K.; Hoggan, M. D.; Martin, M. A.; Orenstein, J. M. J Virol 1990, 64, 621–629.
13. Miller, R. H.; Sarver, N. Nat Med 1997, 3, 389–394.
14. Malim, M. H.; Emerman, M. Cell Host Microbe 2008, 3, 388–398.
15. Greene, W. C.; Peterlin, B. M. Nat Med 2002, 8, 673–680.
16. Willey, R. L.; Maldarelli, F.; Martin, M. A.; Strebel, K. J Virol 1992, 66, 7193–7200.
17. van Damme, N.; Goff, D.; Katsura, C.; Jorgensen, R. L.; Mitchell, R.; Johnson, M. C.; Stephens, E. B.; Guatelli, J. Cell Host Microbe 2008, 3, 1–8.
18. Neil, S. J. D.; Zang, T.; Bieniasz, P. D. Nature 2008, 451, 425–431.

19. Hussain, A.; Wesley, C.; Khalid, M.; Chaudhry, A.; Jameel, S. J Virol 2008, 82, 893–902.
20. Shah, A. H.; Sowrirajan, B.; Davis, Z. B.; Ward, J. P.; Campbell, E. M.; Planelles, V.; Barker, E. Cell Host Microbe 2010, 8, 397–409.
21. Park, S. H.; Mrse, A. A.; Nevzorov, A. A.; Mesleh, M. F.; Oblatt-Montal, M.; Montal, M.; Opella, S. J. J Mol Biol 2003, 333, 409–424.
22. Maldarelli, F.; Chen, M. Y.; Willey, R. L.; Strebel, K. J Virol 1993, 67, 5056–5061.
23. Schubert, U.; Ferrer-Montiel, A. V.; Oblatt-Montal, M.; Henklein, P.; Strebel, K.; Montal, M. FEBS Lett 1996, 398, 12–18.
24. Hussain, A.; Das, S. R.; Tanwar, C.; Jameel, S. Virol J 2007, 4, 1–11.
25. Coady, M. J.; Daniel, N. G.; Tiganos, E.; Allain, B.; Friborg, J.; Lapointe, J.-Y.; Cohen, E. A. Virology 1998, 244, 39–49.
26. Ewart, G. D.; Sutherland, T.; Gage, P. W.; Cox, G. B. J Virol 1996, 70, 7108–7115.
27. Mehnert, T.; Lam, Y. H.; Judge, P. J.; Routh, A.; Fischer, D.; Watts, A.; Fischer, W. B. J Biomol Struct Dyn 2007, 24, 589–596.
28. Mehnert, T.; Routh, A.; Judge, P. J.; Lam, Y. H.; Fischer, D.; Watts, A.; Fischer, W. B. Proteins 2008, 70, 1488–1497.
29. Marassi, F. M.; Ma, C.; Gratkowski, H.; Straus, S. K.; Strebel, K.; Oblatt-Montal, M.; Montal, M.; Opella, S. J. Proc Natl Acad Sci USA 1999, 96, 14336–14341.
30. Wray, V.; Kinder, R.; Federau, T.; Henklein, P.; Bechinger, B.; Schubert, U. Biochemistry 1999, 38, 5272–5282.
31. Henklein, P.; Kinder, R.; Schubert, U.; Bechinger, B. FEBS Lett 2000, 482, 220–224.
32. Wray, V.; Federau, T.; Henklein, P.; Klabunde, S.; Kunert, O.; Schomburg, D.; Schubert, U. Int J Peptide Protein Res 1995, 45, 35–43.
33. Willbold, D.; Hoffmann, S.; Rösch, P. Eur J Biochem 1997, 245, 581–588.
34. Coadou, G.; Evrard-Todeschi, N.; Gharbi-Benarous, J.; Benarous, R.; Girault, J.-P. C R Acad Sci – Series IIC – Chemistry 2001, 4, 751–758.
35. Ma, C.; Marassi, F. M.; Jones, D. H.; Straus, S. K.; Bour, S.; Strebel, K.; Schubert, U.; Oblatt-Montal, M.; Montal, M.; Opella, S. J. Prot Sci 2002, 11, 546–557.
36. Wittlich, M.; Koenig, B. W.; Stoldt, M.; Schmidt, H.; Willbold, D. FEBS J 2009, 276, 6560–6575.
37. Krüger, J.; Fischer, W. B. J Comp Chem 2008, 29, 2416–2424.
38. Fink, A.; Sal-Man, N.; Gerber, D.; Shai, Y. Biochim Biophys Acta 2012, 1818, 974–983.
39. Moore, P. B.; Zhong, Q.; Husslein, T.; Klein, M. L. FEBS Lett 1998, 431, 143–148.
40. Cordes, F.; Kukol, A.; Forrest, L. R.; Arkin, I. T.; Sansom, M. S. P.; Fischer, W. B. Biochim Biophys Acta 2001, 1512, 291–298.
41. Kukol, A.; Arkin, I. T. Biophys J 1999, 77, 1594–1601.
42. Krüger, J.; Fischer, W. B. J Chem Theory Comput 2009, 5, 2503–2513.
43. Hsu, H.-J.; Fischer, W. B. J Mol Mod 2011, 18, 501–514.
44. Imoto, K. FEBS Lett 1993, 325, 100–103.
45. Hilf, R. J. C.; Dutzler, R. Nature 2008, 452, 375–379.
46. Hilf, R. J. C.; Dutzler, R. Nature 2009, 457, 115–119.
47. Grice, A. L.; Kerr, I. D.; Sansom, M. S. P. FEBS Lett 1997, 405, 299–304.
48. Cordes, F. S.; Tustian, A. D.; Sansom, M. S.; Watts, A.; Fischer, W. B. Biochemistry 2002, 41, 7359–7365.
49. Patargias, G.; Martay, H.; Fischer, W. B. J Biomol Struct Dyn 2009, 26, 1–12.
50. Lopez, C. F.; Montal, M.; Blasie, J. K.; Klein, M. L.; Moore, P. B. Biophys J 2002, 83, 1259–1267.
51. Lu, J.-X.; Sharpe, S.; Ghirlando, R.; Yau, W.-M.; Tycko, R. Prot Sci 2010, 19, 1877–1896.
52. Lee, J.; Chen, J.; Brooks III, C. L.; Im, W. J Magn Res 2008, 193, 68–76.
53. Griffin, S. D. C.; Beales, L. P.; Clarke, D. S.; Worsfold, O.; Evans, S. D.; Jäger, J.; Harris, M. P. G.; Rowlands, D. J. FEBS Lett 2003, 535, 34–38.
54. Luik, P.; Chew, C.; Aittoniemi, J.; Chang, J.; Wentworth Jr., P.; Dwek, R.; Biggin, P. C.; Vénien-Bryan, C.; Zitzmann, N. Proc Natl Acad Sci USA 2009, 106, 12712–12716.
55. Clarke, D.; Griffin, S.; Beales, L.; Gelais, C. S.; Burgess, S.; Harris, M.; Rowlands, D. J Biol Chem 2006, 281, 37057–37068.
56. Sharpe, S.; Yau, W. M.; Tycko, R. Biochemistry 2006, 45, 918–933.
57. Krüger, J.; Fischer, W. B. Eur Biophys J 2010, 39, 1069–1077.
58. Cornell, W. D.; Cieplak, P.; Bayly, C. I.; Gould, I. R.; Merz Jr., K. M.; Ferguson, D. M.; Spellmeyer, D. C.; Fox, T.; Caldwell, J. W.; Kollman, P. A. J Am Chem Soc 1995, 117, 5179–5197.
59. Schäfer, L. V.; de Jong, D. H.; Holt, A.; Rzepiela, A. J.; de Vries, A. H.; Poolman, B.; Killian, J. A.; Marrink, S. J. Proc Natl Acad Sci USA 2011, 108, 1343–1348.
60. Ruiz, A.; Hill, M. S.; Schmitt, K.; Stephens, E. B. Virology 2010, 408, 89–102.
61. Efremov, R. G.; Vereshaga, Y. A.; Volynsky, P. E.; Nolde, D. E.; Arseniev, A. S. J Comput Aided Mol Des 2006, 20, 27–45.
62. Bond, P. J.; Sansom, M. S. P. J Am Chem Soc 2006, 128, 2697–2704.
63. Vereshaga, Y. A.; Volynsky, P. E.; Pustovalova, J. E.; Nolde, D. E.; Arseniev, A. S.; Efremov, R. G. Proteins: Struct Funct Genet 2007, 69, 309–325.
64. Bu, L.; Im, W.; Brooks C. L. III. Biophys J 2007, 92, 854–863.
65. Psachoulia, E.; Marshall, D. P.; Sansom, M. S. P. Acc Chem Res 2010, 43, 388–396.
66. Yin, H.; Slusky, J. S.; Berger, B. W.; Walters, R. S.; Vilaire, G.; Litvinov, R. I.; Lear, J. D.; Caputo, G. A.; Bennett, J. S.; DeGrado, W. F. Science 2007, 315, 1817–1823.
67. Beckstein, O.; Biggin, P. C.; Sansom, M. S. P. J Phys Chem B 2001, 105, 12902–12905.
68. Beckstein, O.; Sansom, M. S. P. Phys Biol 2006, 3, 147–159.
69. Skasko, M.; Wang, Y.; Tian, Y.; Tokarev, A.; Munguia, J.; Ruiz, A.; Stephens, E. B.; Opella, S. J.; Guatelli, J. J Biol Chem 2012, 287, 58–67.

Reviewing Editor: Stephen Blacklow